Recent Results from the BRAHMS Experiment

P. Staszel[a] (for the BRAHMS Collaboration)*

[a]Jagiellonian University, Institute of Physics,
ul. Reymonta 4, 30-059 Kraków, Poland

We present results obtained by the BRAHMS experiment at the Relativistic Heavy Ion Collider (RHIC) for four colliding systems, namely: Au + Au and Cu + Cu at $\sqrt{s_{NN}} = 200$ GeV and $\sqrt{s_{NN}} = 62.4$ GeV, and d + Au and p + p at $\sqrt{s_{NN}} = 200$ GeV. The focus here is to give an overview of the main results on the reaction dynamics and on the properties of hot and high energy density matter produced in utra-relativistic heavy ion collisions versus its longitudinal expansion. Measurement of particle production, particle spectra over a large rapidity interval as well as high p_T measurements related to nuclear modification in Au + Au and Cu + Cu and d + Au collision are discussed. The observed number of charged particles produced per unit of rapidity at the central rapidity region indicates that a high energy density systems are created at the initial stage of the Au + Au reaction. Analysis of anti-particle to particle ratios (including multi-strange baryon) as the function of rapidity and collision energy reveals that particles population at the chemical freeze-out stage for heavy ion reaction at and above SPS energies is controlled only by baryon chemical potential. From the particle spectra we deduced significant radial expansion ($\beta \approx 0.75$) which is consistent with the large initial energy density. We also measured the elliptic flow parameter v_2 versus rapidity and p_T . The weak dependency (if any) of the $v_2(p_T)$ is observed. We present rapidity dependent p/π rations in $0 < y < 3$ for Au + Au and Cu + Cu $\sqrt{s_{NN}} = 200$ GeV. The strong enhancement of proton and anti-proton yields compared to pion yields is seen, and the results are discuss in terms of collision energy, system size and rapidity dependency. We compare R_{AA} for Au + Au at $\sqrt{s_{NN}} = 200$ GeV and $\sqrt{s_{NN}} = 62.4$ GeV, and for Au + Au and Cu + Cu at $\sqrt{s_{NN}} = 200$ GeV. The general observed trend is that R_{AA} increases with: decreasing collision energy, system size, and collision centrality. R_{AA} shows very weak dependency on rapidity (in $0 < y < 3.2$ interval), both for pions and protons.

1. INTRODUCTION

Reactions between heavy nuclei provides a unique opportunity to produce and study nuclear (hadronic) matter far from its ground state, at extremely high densities and temperatures. From the onset of the formulation of the quark model and the first understanding of the nature of the binding and confining potential between quarks about 30 years ago, it has been realized that at very high density and temperature the hadronic

*For the full BRAHMS Collaboration author list and acknowledgment see appendix 'Collaborations' of this volume

matter may undergo transition to the more primordial form of matter characterized by a strongly reduced interaction between its constituents, quarks and gluons, such that the partons would exist in the nearly free state [**?**]. This proposed state of matter has been named the quark gluon plasma (QGP).

Experimental attempts to create the QGP in the laboratory by colliding heavy nuclei have been carried out for more than 20 years. During that period, center of mass energies per pair of colliding nucleons have risen steadily from the $\sqrt{s_{NN}} = 1$ GeV domain of the Bevalac at LBNL, to energies of $\sqrt{s_{NN}} = 5$ GeV at the AGS at BNL, and to $\sqrt{s_{NN}} = 17$ GeV at the SPS at CERN. Although a number of signals suggesting the formulation of a very dense state of matter have been observed, no strong evidence for QGP formation was found at these energies.

In mid-August 2001 systematic data collecting by the four RHIC experiments, namely BRAHMS, PHENIX, PHOBOS and STAR, began at the energy of $\sqrt{s_{NN}} = 200$ GeV. The RHIC operations started a new era of systematic studies of strongly interacting matter created in ultra-relativistic nucleus-nucleus collision. The main results obtained up to present at RHIC are the large eliptic flow observed for central Au + Au collisions, that is consistent with the hydrodynamic evolution of the perfect fluid [1–3], and the strong jet suppression [5] predicted within the Quantum Chromo-Dynamic theory, (QCD), as a consequence of creation of the dense colored medium [6]. The last observation was supplemented by d + Au measurement showing absence of suppression, and rather Cronin type enhancement at the central rapidity region that excluded alternative interpretation of suppression in terms of initial state parton saturation (CGC) effects. Another measurement that strongly supported the scenario of jet quenching was the discovery of mono-jet production [7,8] in central Au + Au collisions, whereas, for d + Au and peripheral Au + Au near side and away side back-to-back jet correlation have been measured. The large rapidity range and p_T coverage allows BRAHMS to study the properties of the produced medium as a function of its longitudinal expansion. The measurement of rapidity evolution of the nuclear modification factor for d + Au performed by BRAHMS shown that at more forward rapidities the hadronic yields are suppressed as compared to scaled p + p interactions [9]. The suppression was even stronger for central collisions. Both observations can be quantitatively described within the framework of CGC [6,10].

2. BRAHMS DETECTOR SETUP

The BRAHMS (Broad RAnge Hadron Magnetic Spectrometers) [11], experimental setup consists of a set of global detectors and two spectrometer arms: Mid-Rapidity Spectrometer (MRS) that operates in the polar angle range from 30 to 95 degrees, and the Forward Spectrometer (FS) that operates in the range between 2 and 30 degrees. Global detectors can measure the global features of the collision like overall particle multiplicity and centrality, collision vertex position, and recently they provide also information on reaction plane orientation utilized in the azimuthal flow analysis. For the momentum measurements in the MRS we use two tracking devices and one dipol magnet. Particle identification (PID) is done by the Time of Flight (TOF) measurement and using Cherenkov detector C4. In the FS two Time Projection Chambers (TPC) and three Drift Chambers (DC) deliver particle track segments and for the momentum measurement we

use three dipol magnets. The PID is provided by TOF measurements for low (TOF1) and medium (TOF2) particle momenta, and by the Ring Imaging Cherenkov detector (RICH) in the high momentum mode measurement. The BRAHMS PID ability is summarized in Table 1.

Table 1
Upper range of the momentum for 2σ separation (in GeV/c)

	$0 < \eta < 1.0$			$1.5 < \eta < 4.0$		
	TOFW	TOFW2	C4	TOF1	TOF2	RICH
K/π	2.0	2.5	-	3.0	4.5	25.0
K/p	3.5	4.0	9.0	5.5	7.5	35.0

3. OVERALL BULK CHARACTERISTICS

The multiplicity distribution of emitted particles is a fundamental observable in ultra-relativistic collisions. It is sensitive to all stages of the reaction and can address issues like the role of hard scatterings between partons and the interaction of these partons in the high-density medium [12–14]. Figure 1 shows the measured pseudo-rapidity density of charged hadrons, $\mathrm{dN}_{ch}/\mathrm{d}\eta$, over a wide range of η for the central $(0-5\%)$ Au + Au collisions at $\sqrt{s_{NN}} = 200$ GeV, $\sqrt{s_{NN}} = 130$ GeV and $\sqrt{s_{NN}} = 62.4$ GeV. For the central collisions at $\sqrt{s_{NN}} = 200$ GeV we observed about 4500 of charged particles within the rapidity range covered and the $\mathrm{dN}_{ch}/\mathrm{d}\eta \mid_{\eta=0} = 625 \pm 56$. The latter value exceeds the particle production per participant pair observed in elementary p + $\bar{\mathrm{p}}$ collisions at the same energy by 40-50% [15]. This means that nucleus-nucleus collisions at the considered energies are far from being the simple superposition of elementary collisions.

This simple measurement of charged particle density $dN_{ch}/d\eta$ can be used to estimate the so-called Bjorken energy density, ε [16]. The formula

$$\varepsilon = \frac{3}{2} \times \frac{\langle E_t \rangle}{\pi R^2 \tau_o} \times \frac{dN_{ch}}{d\eta} \tag{1}$$

provides the value of about 4 GeV/fm^3. To obtained this result we assumed that $\tau_o = 1$ fm/c, $\langle E_t \rangle = 0.5$ GeV and R = 6 fm. The factor 3/2 is due to the assumption that the charged particles carried out of the reaction zone only a fraction (2/3) of the total available energy. The more refined results obtained from the identified particle abundances and particle spectra leads to somewhat larger values of ε, namely 5 GeV/fm^3 at $\sqrt{s_{NN}} =$ 200 GeV, 4.4 GeV/fm^3 at $\sqrt{s_{NN}} = 130$ GeV, and 3.7 GeV/fm^3 at $\sqrt{s_{NN}} = 62.4$ GeV, [17]. All these values significantly exceed the predicted energy density $\varepsilon \approx 1$ GeV/fm^3 for the boundary between hadronic and partonic phases [18].

3.1. Hadrochemistry with BRAHMS data

BRAHMS measurements allow to derive the anti-particle to particle ratios for pions, N_{π^-}/N_{π^+}, kaons, N_{K^-}/N_{K^+}, and protons, $N_{\bar{\mathrm{p}}}/N_{\mathrm{p}}$, over the large rapidity interval. The

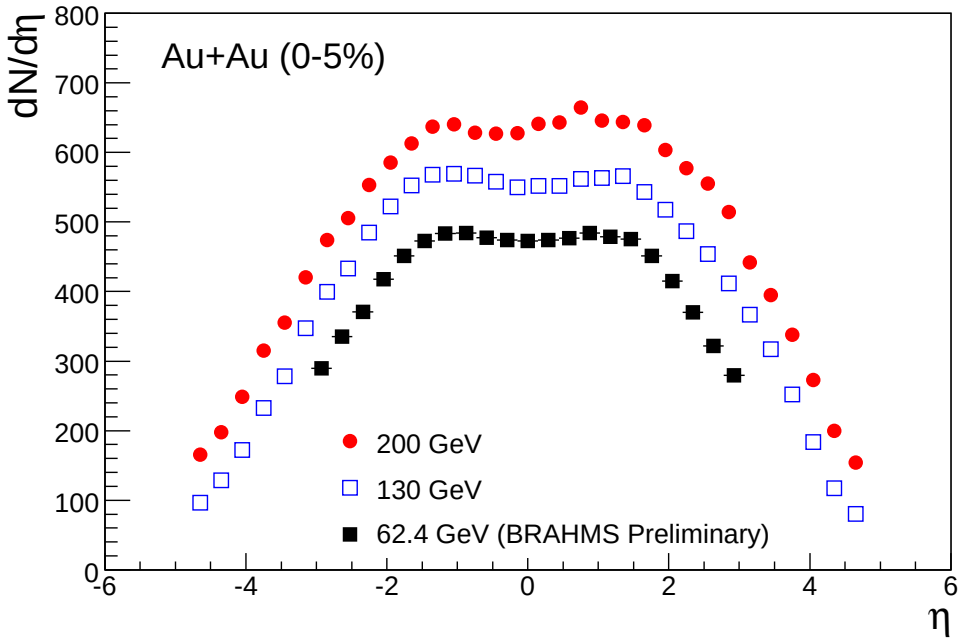

Figure 1. Distributions of $dN_{ch}/d\eta$ measured by BRAHMS for $0-5\%$ central Au + Au reactions, at $\sqrt{s_{NN}} = 200$ GeV (solid circles), $\sqrt{s_{NN}} = 130$ GeV (open squares) and $\sqrt{s_{NN}} = 62.4$ GeV (solid squares). Only statistical error (usually smaller than the symbol size) are shown.

results, for Au + Au collision at $\sqrt{s_{NN}} = 200$ GeV and $\sqrt{s_{NN}} = 62.4$ GeV are presented on Figure 2. Whereas N_{π^-}/N_{π^+} stays constant and is equal 1 in the whole covered rapidity range ($0 < \mathrm{y} < 3.2$) for all RHIC energies, the N_{K^-}/N_{K^+} and $N_{\bar{\mathrm{p}}}/N_{\mathrm{p}}$ drop significantly with increasing rapidity. For $\sqrt{s_{NN}} = 200$ GeV the N_{K^-}/N_{K^+} and $N_{\bar{\mathrm{p}}}/N_{\mathrm{p}}$ equal respectively 0.95 and 0.76 at $y \approx 0$, and reach values of 0.6 for N_{K^-}/N_{K^+} and 0.3 for $N_{\bar{\mathrm{p}}}/N_{\mathrm{p}}$ around rapidity 3. Comparing $\sqrt{s_{NN}} = 200$ GeV and $\sqrt{s_{NN}} = 62.4$ GeV we observe 11% and 40% decrease of ratios at mid-rapidity and 43% and 93% decrease at $y \approx 3$ for kaons and protons, respectively. The large difference in the $N_{\bar{\mathrm{p}}}/N_{\mathrm{p}}$ reduction for $\sqrt{s_{NN}} = 200$ GeV and $\sqrt{s_{NN}} = 62.4$ GeV is due to the fact that for the lower energy the rapidity $y \approx 3$ corresponds to the fragmentation region, whereas for $\sqrt{s_{NN}} = 200$ GeV $y \approx 3$ is located about 1 unit of rapidity below the maximum in the net-baryon distribution [19].

Figure 3 shows the N_{K^-}/N_{K^+} as a function of corresponding $N_{\bar{\mathrm{p}}}/N_{\mathrm{p}}$ for various rapidities. The data are for central collisions for the three studied collision energies studied at RHIC. The AGS and SPS results are plotted for comparison. There is a striking correlation between the RHIC/BRAHMS kaon and proton ratios over 3 units of rapidity. It is worth to note that the BRAHMS forward rapidity data measured at $\sqrt{s_{NN}} = 62.4$ GeV overlap with the SPS points that were measured at much lower energy but at mid-rapidity. The solid line plotted on the figure refers to the fit with a statistical model to the $\sqrt{s_{NN}} = 200$ GeV results assuming that the temperature at the chemical freeze-

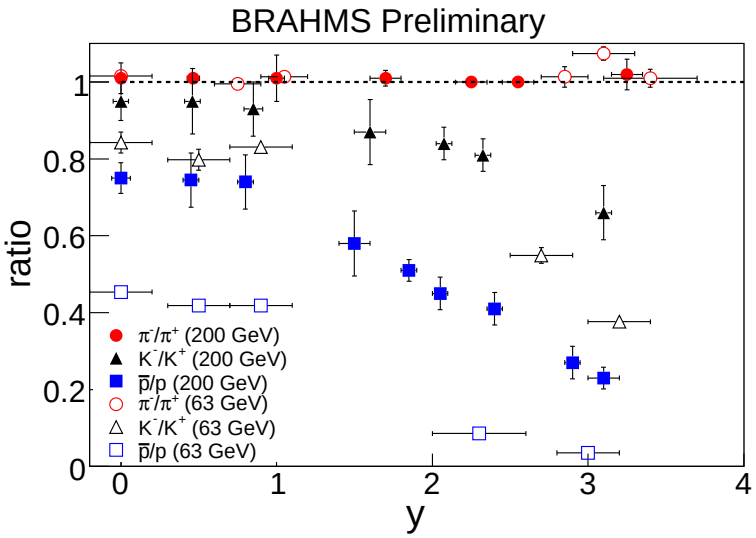

Figure 2. Ratios of anti-particles to particles (pions, kaons and protons) at a function of rapidity for $\sqrt{s_{NN}} = 62.4$ GeV, $\sqrt{s_{NN}} = 200$ GeV. Statistical and systematic errors are indicated.

out is 170 MeV [20,21]. It is seen that the data are very well described by the statistical model over the broad rapidity range with baryonic chemical potential changing from 27 MeV at mid-rapidity to 140 MeV at the most forward rapidities. Using simple statistical model at the quark level with chemical and thermal equilibrium, the ratios can be written

$$\frac{N_{\bar{p}}}{N_p} = e^{-6\mu_{u,d}/T}, \qquad \frac{N_{K^-}}{N_{K^+}} = e^{-2(\mu_{u,d}-\mu_s)/T}, \tag{2}$$

where μ and T are chemical potential and temperature, respectively. Substituting $\mu_s = 0$ into eqs. (2), one gets $N_{K^-}/N_{K^+} = [N_{\bar{\mathrm{p}}}/N_{\mathrm{p}}]^{1/3}$. This relation, represented by the dotted line on Figure 3, does not reproduce the observed correlation. The data are however well fitted by the function $N_{K^-}/N_{K^+} = [N_{\bar{\mathrm{p}}}/N_{\mathrm{p}}]^{1/4}$ (dashed line) which can be derived from eqs. (2) assuming $\mu_s = 1/4\mu_{u,d}$.

Recently, STAR and NA49 have measured mid-rapidity ratios $\bar{\Lambda}/\Lambda$, $\bar{\Xi}/\Xi$ and $\bar{\Omega}/\Omega$ versus $N_{\bar{\mathrm{p}}}/N_{\mathrm{p}}$ for set of energies from $\sqrt{s_{NN}} = 10$ GeV up to $\sqrt{s_{NN}} = 200$ GeV. These preliminary results can also be well discribed within statistical model of chemical and thermal equilibrium at the quark level and confirm the the strong correlation between μ_s and $\mu_{u,d}$ derived from BRAHMS data.

3.2. Radial flow

The properties of matter in the latest stage of the collision when the interactions between particles cease (kinetic freeze-out) can be studied from the shape of spectra of the emitted particles. This shape depends in general on the temperature of the emitting source and on the collective flow. For central collisions where one should not expect any azimuthal dependency only the so-called transverse (radial) flow is important [3]. In the blast-wave approach [22] the spectrum is parametrized by a function depending on the freeze-out temperature, (T_{fo}), and on the transverse expansion velocity (β_T). Figure 4 shows results from analysis of the particle spectra from the Au + Au reaction at

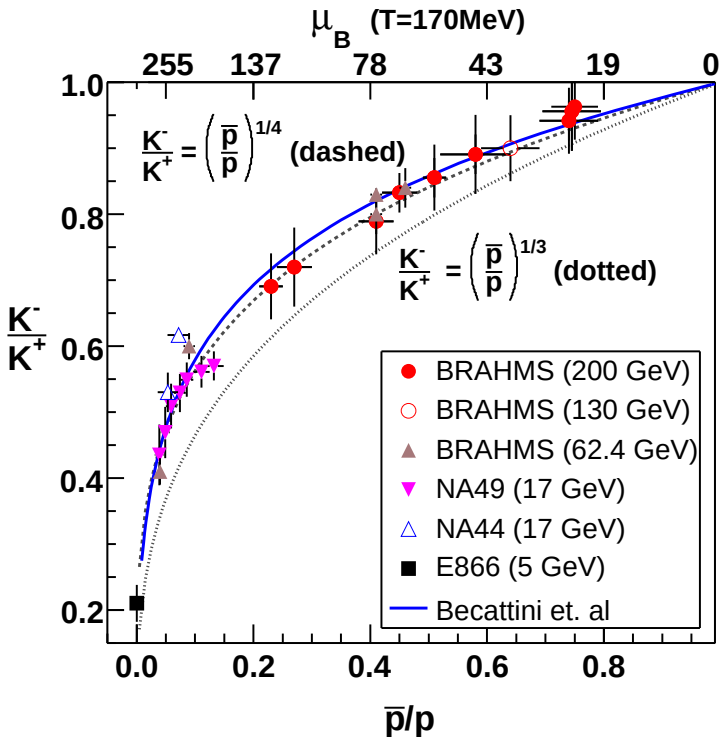

Figure 3. Correlation between $N_{K^-}/N_{K^+}$and $N_{\bar{\mathrm{p}}}/N_{\mathrm{p}}$. The solid curve refer to statistical model calculation with a chemical freeze-out temperature of 170 MeV.

$\sqrt{s_{NN}}$ = 200 GeV using the blast-wave model fit, simultaneously to π^+, π^-, K^+,K^-, protons and anti-protons, plotted versus number of participant pairs (N_{part}).

The obtained result indicates that the kinetic freeze-out temperature decreases with centrality from about 140 MeV for $40-50\%$ centrality bin to about 120 MeV for the most central collisions. The second quantity is lower than the temperature of the chemical freeze-out indicating that, as expected, the freeze-out of particle ratios occurs earlier than the kinetic freeze-out. The reversed trend is seen for the expansion velocity which is equal about 0.65c and 0.75c for $40-50\%$ centrality and $0-5\%$ centrality class, respectively. For comparison we show also the results for Au + Au collisions at $\sqrt{s_{NN}}$ = 62.4 GeV. Although for the same N_{part} value the T_{fo} for both energies is very similar, the reduction by about 20% in the expansion velocity is observed.

Figure 5 shows the dependence of T_{fo} and β_T as a function of rapidity. The observed variations of T_{fo} and β_T on N_{part} and rapidity are consistent with the hydrodynamic description in which the radial flow is the result of outwards gradients of pressure that exists in the expanding matter during the whole evolution. Thus the speed of expansion should increase with the density of the initially created system. The transverse flow velocity is larger than that observed at SPS energies what is consistent with a large initial density of the system created at RHIC.

3.3. Elliptic Flow

The powerful tool to study the dynamic that drives the initial evolution of systems created in heavy ion reactions is the analysis of the azimuthal distribution of the emitted

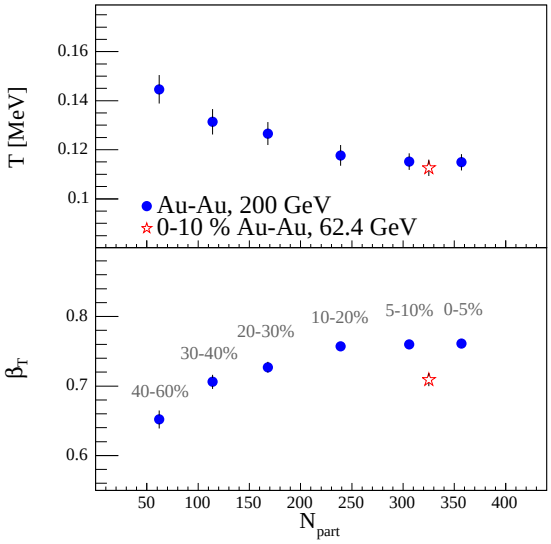

Figure 4. Kinetic freeze-out temperature and transverse flow velocity at mid-rapidity as a function of centrality for Au + Au at $\sqrt{s_{NN}}$ = 200 GeV (dots). For the comparison we show result for $0-10\%$ central Au + Au at $\sqrt{s_{NN}} = 62.4$ GeV (star).

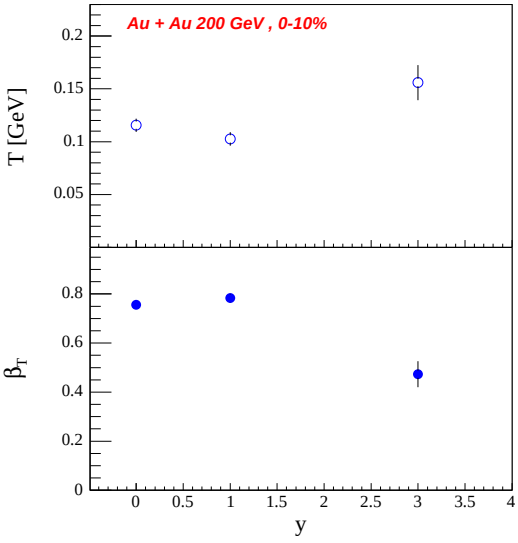

Figure 5. Kinetic freeze-out temperature and transverse flow velocity for central Au + Au at $\sqrt{s_{NN}} = 200$ GeV as a function of rapidity.

particles relative to the reaction plane [3]. The triple differential distribution of emitted particles can be factorized as follow

$$\frac{dN}{dydp_Td\phi} = \frac{dN}{dydp_T}\frac{1}{2\pi} \times (1 + 2v_1(y,p_T)cos(\phi - \phi_r) + 2v_2(y,p_T)cos2(\phi - \phi_r) + ...). \quad (3)$$

where ϕ and ϕ_r denote the azimuthal angles of the particle and of the reaction plane, respectively. The first factor depends only on y and p_T and the second factor represents the expansion of the azimuthal dependence into the Fourier series. The coefficients at the first (v_1) and the second (v_2) harmonics are called direct and elliptic flow parameter, respectively, and in general they are functions of rapidity and transverse momentum. The calculations based on hydrodynamic models [3] show that the elliptic flow is substantially generated only during the highest density phase, before the initial spatial anisotropy of created medium disappears. Thus v_2 is sensitive to the very early phase in the system evolution and relatively insensitive to the late stage characterized by the dissipative expansion of the hadronic gas.

Elliptic flow has been extensively measured by the STAR, PHENIX and PHOBOS experiments [1,2,4]. Generally, the v_2 is an increasing function of p_T up to 1.5 GeV/c, at which point it saturates. Up to roughly 1.5 GeV/c in p_T , hydrodynamic calculations show good agreement with experimental data for the v_2 dependence on p_T and centrality.

BRAHMS has measured the p_T dependence of v_2 at set of rapidities [23], and the results for pions at $\eta = 0$ and at $\eta = 3.4$ are shown on Figure 6. v_2 for identified pions

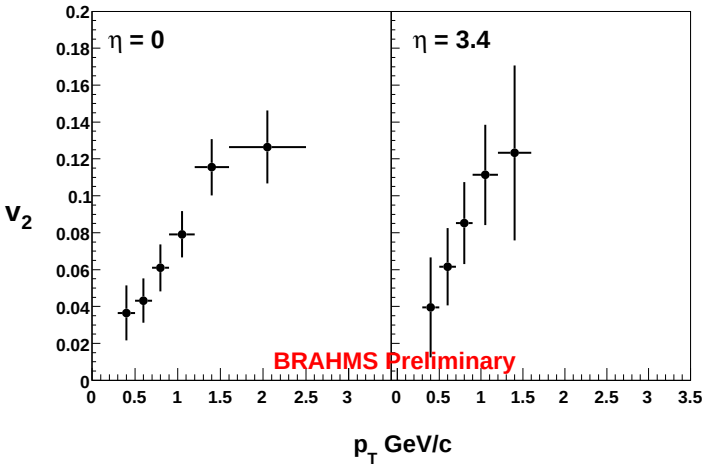

Figure 6. Pion elliptic flow parameter p_T dependence measured for Au + Au at $\sqrt{s_{NN}}$ = 200 GeV at $\eta = 0$ and at $\eta = 3.2$.

is an increasing function of p_T at both rapidities, with indication of saturation above 1.5 GeV/c. The dependence on pseudo rapidity is very small. These results are very similar to that obtained for charged hadrons [23].

4. BARYON TO MESON RATIOS

With its excellent particle identification capabilities BRAHMS can study the p_T and y dependency for different type of hadrons production. Preliminary results [24,25] indicate that for Au + Au reactions in the intermediate p_T region the proton to meson ratio is significantly higher that one would expect from the parton fragmentation in vacuum. Several theoretical explanations in terms of partonic interactions like models of quark hadronization and quark coalescence [26–28] and models that incorporate the novel baryon dynamics [29,30] have been proposed. The recent experimental data obtained for the p + p, Au + Au, and Cu + Cu colliding systems are expected to result in a better understanding of the underlying physics and verification of the proposed theoretical scenarios. Fig. 7 shows a recent investigation by BRAHMS [31], of the $\bar{p}$ to π^- ratios at mid-rapidity (circles) and at pseudo rapidity $\eta = 3.2$ (squares) for Au + Au collisions at $\sqrt{s_{NN}} = 200$ GeV for different centrality classes indicated on the plot. The bottom panel shows the ratios for p + p at $\sqrt{s_{NN}} = 200$ GeV measured by PHENIX at mid-rapidity and by BRAHMS at forward rapidity. The data reveal smooth increase of $\bar{p}/\pi^-$ from peripheral to central collisions, however, the centrality dependence is stronger at mid-rapidity than at forward rapidity. The maxima in $\bar{p}/\pi^-$ ratio is lower at forward rapidity as compared to mid-rapidity. Figure 8 shows the $\bar{p}/\pi^-$ centrality dependence for Au + Au (open symbols) and Cu + Cu (solid symbols) at $\sqrt{s_{NN}} = 200$ GeV. The data for $y = 0$ and $\eta = 3.2$ are represented by circles and squares, respectively. One can see the strong increase of $\bar{p}/\pi^-$ as a functon of N_{part} in the range from 0 to 100. For $N_{part} > 100$ the dependence saturates and the ratios reach values of about 0.6 and about 0.25 for mid and forward rapidity, respectively. For peripheral Au + Au collisions the data approach the

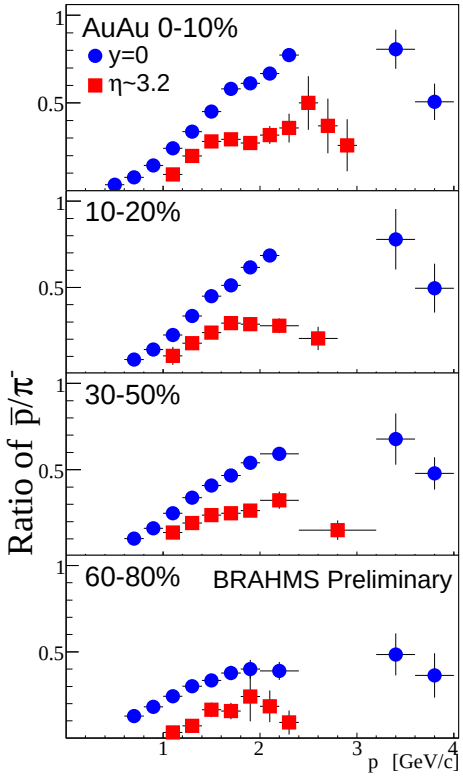

Figure 7. The $\bar{p}$ to π^- ratios at mid-rapidity (circles) and at pseudo rapidity $\eta = 3.2$ (squares) for different centralities of Au + Au collisions at $\sqrt{s_{NN}} = 200$ GeV.

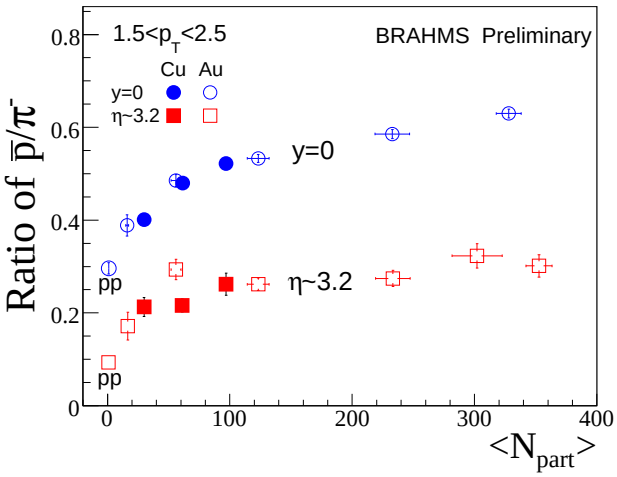

Figure 8. The averaged $\bar{p}/\pi^-$ versus N_{part} for Au + Au (open symbols) and Cu + Cu (solid symbols) at $\sqrt{s_{NN}} = 200$ GeV, for $y \approx 0$ (circles) and and for $\eta \approx 3.2$ (squers).

p + p results. It is important to note that the Au + Au and Cu + Cu ratios are consistent with each other when plotted versus N_{part} what indicates that the enhancement of $\bar{p}$ over π^- is controlled by the initial size of the created systems. Fig. 9 shows the comparison of BRAHMS and PHENIX data for the ratio of protons to positive pions measured at $y = 0$ with the theoretical calculation. The parton coalescence [27] and recombination [28] models describe the observed ratios well at mid-rapidity. The three-dimentional hydrodynamic model [32] can not reproduce the observed shape of p/π^+, however it reproduces the overall level of enhancement. The current hydrodynamic calculations do not show a rapidity depencence which is in contrary to the experimental observation (see Fig. 9). This is presumably because the baryon and isospin chemical potentials are not included in this model.

5. HIGH p_T SUPPRESSION

Particles with high p_T (above 2 GeV/c) are primarily produced in hard scattering processes early in the collision. In high energy nucleon-nucleon reactions hard scattered partons fragment into jets of hadrons. However, in nucleus-nucleus collision hard scattered

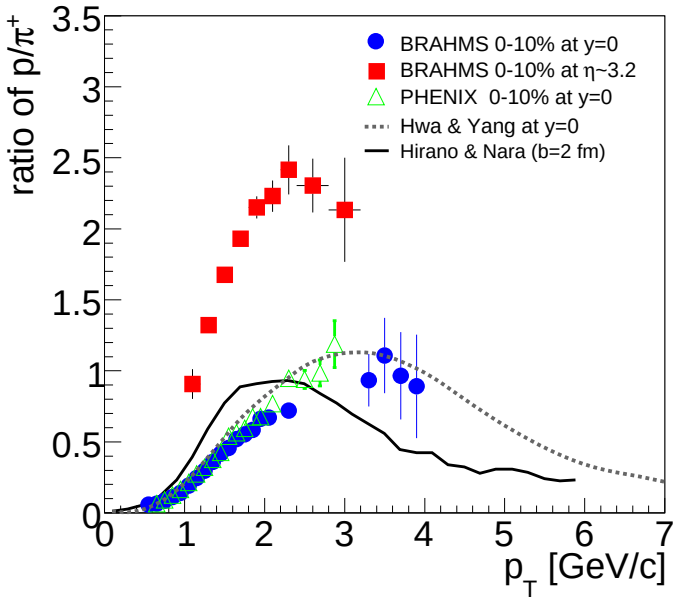

Figure 9. The p/π^+ versus p_T for Au + Au collisions at $\sqrt{s_{NN}}$ = 200 GeV measured at mid-rapidity by BRAHMS (circles) and by PHENIX (triangles). Squares represent BRAHMS results at $eta = 3.2$. The plotted lines show model calculations (see text).

partons might travel in the medium. It was predicted that, if the medium is QGP, the partons will lose a large fraction of their energy by induced gluon radiation, effectively leading to suppression of jet production [33]. Experimentally this phenomenon, known as jet quenching, will be observed as a depletion of the high p_T region in hadron spectra.

The measure commonly used to study the medium effects is called the nuclear modification factor, R_{AA} . It is defined as a ratio of the particle yield produced in nucleus-nucleus collision, scaled with the number of binary collisions (N_{coll}), and the particle yield produced in elementary nucleon-nucleon collision

$$R_{AA} = \frac{Yield(AA)}{N_{coll} \times Yield(NN)}. \tag{4}$$

At high p_T the particles are predominantly produced by hard scatterings and in the absence of nuclear effects (when the nucleus-nucleus collision reduces to the superposition of elementary collisions) we expect R_{AA} to be 1. At low p_T , where the production rate scales rather with N_{part} , R_{AA} should converge to N_{part}/N_{coll} which is roughly 1/3 for central Au + Au at RHIC energies. $R_{AA} < 1$ at high p_T will indicate the suppression which, as has been discussed, is consistent with the jet quenching phenomenon. At SPS there is no suppression, in fact it is well known that there is enhancement for p_T > 2 GeV/c and this so-called Cronin effect is attributed to initial multiple scattering of reacting partons.

Another variable used to quantify nuclear effects, that does not depend on the elementary reference spectra, is R_{CP} , defined as a ratio of R_{AA} at central nucleus-nucleus collisions to R_{AA} at peripheral collisions. The idea of using R_{CP} bases on the expectation

Figure 10. R_{AA} measured at $\eta \approx 0$ and $\eta \approx 1$ for Au + Au at $\sqrt{s_{NN}} = 200$ GeV (upper row) and at $\sqrt{s_{NN}} = 62.4$ GeV (bottom row), for different centrality classes indicated on the plot. (p + p reference is based on ISR collider data)

that any nuclear modification in peripheral collisions in not significant. We will show that the latter statement is not true for $R_{CP} = R_{AuAu}(0-10\%)/R_{AuAu}(40-60\%)$.

5.1. R_{AA} evolution on collision centrality and collision energy for Au + Au and Cu + Cu systems

The large set of data collected during the RHIC run 4 has allowed us to carry out the study of the R_{AA} evolution on collision centrality and collision energy for two colliding systems, namely Au + Au and Cu + Cu [34]. Figure 10 shows R_{AA} measured at $\eta \approx 0$ and $\eta \approx 1$ for Au + Au at $\sqrt{s_{NN}} = 200$ GeV (upper row) and at $\sqrt{s_{NN}} = 62.4$ GeV (bottom row), for different centrality ranges indicated on the plot. For the most central reactions the R_{AA} shows suppression for both energies, however, the suppression is significantly stronger for the system colliding with higher energy. We observe a smooth increase of R_{AA} towards less central collisions, for $\sqrt{s_{NN}} = 200$ GeV, resulting in approximate scaling with N_{coll} for $p_T > 2$ GeV/c for $40-50\%$ centrality bin. However, at $\sqrt{s_{NN}} = 62.4$ GeV scaling appears for more central collisions, and the Cronin peak in clearly visible already for $20-40\%$ centrality class, where R_{AA} reaches value of about 1.3 in the p_T range between 2.0 and 3.0 GeV/c. This observations are qualitatively consistent with the picture in which there are two competing mechanisms that influence the nuclear modification in the intermediate and high p_T range, namely: the jet quenching that dominates at central collisions and Cronin type enhancement (k_T broadening or/and quark recombination) that prevails for the more peripheral collisions.

The next figure (Fig. 11), presents similar comparison as shown on Fig. 10 but this time we compare two different systems, namely Au + Au and Cu + Cu colliding at the same energy ($\sqrt{s_{NN}} = 62.4$ GeV). For Cu + Cu at $\sqrt{s_{NN}} = 62.4$ GeV the same trend of increasing R_{AA} with decreasing collision centrality is seen, however, the Cronin type enhancement is present already for the most central collisions.

Summarizing the whole set of observation we conclude that the level of suppression of the inclusive hadron spectra produced in the nucleus-nucleus collisions at RHIC energies in the p_T range above 2 GeV increases with increasing collision energy, collision centrality and with the size of the colliding nuclei. The dependency on the last two variables can

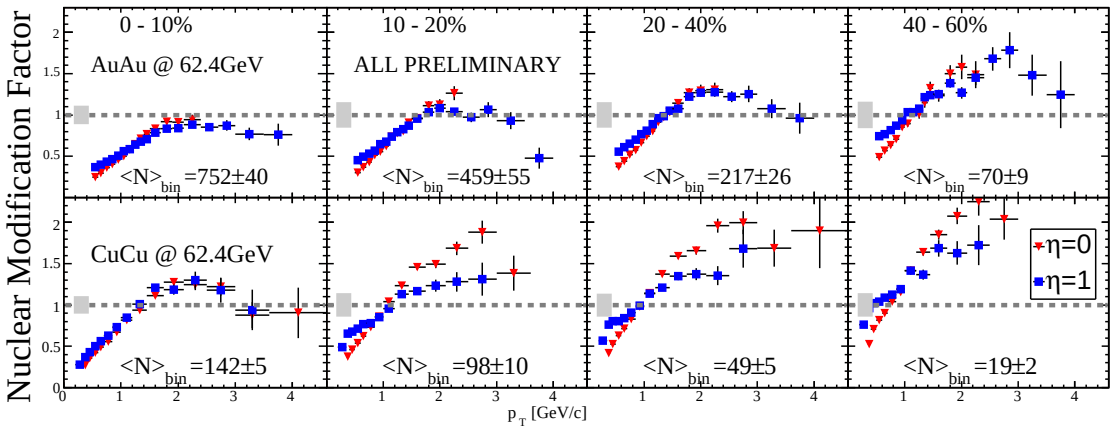

Figure 11. R_{AA} measured at mid-rapidity for Au + Au (upper row) and for Cu + Cu (bottom row) at $\sqrt{s_{NN}} = 62.4$ GeV for different centrality classes indicated on the plot. (p + p reference is based on ISR collider data)

be replaced by only one dependency on N_{part} .

PS comment: we haven't shown the direct argument for what is stated in the last sentence but plotting R_{AA} versus N_{part} for (Au+Au and CuCu at 62) maybe would show that? It looks like it can be done for eta=1.

5.2. R_{AA} for identified hadrons at forward rapidity for Au + Au at $\sqrt{s_{NN}} =$ 200 GeV

BRAHMS collaboration has already announced a large suppression of the nuclear modification factor (similar to that seen at mid-rapidity) measured at large pseudo rapidity of $\eta = 2.2$ in Au + Au at $\sqrt{s_{NN}} = 200$ GeV [5]. However, the data did not allow to verify the mechanism responsible for the observed effect. In this section we present more exclusive analysis of nuclear effects at forward rapidity for identified pions, kaons and protons.

Figure 12 shows R_{AA} for identified hadrons at rapidity $y \approx 3.2$ for $0 - 10\%$ central Au + Au events at $\sqrt{s_{NN}} = 200$ GeV. The shaded band around unity indicates systematic error associated with the uncertainty in the number of binary collisions. Both R_{AA} and R_{CP} show suppression for pions (left panel) and for kaons (middle panel), however protons (right panel) R_{CP} shows suppression whereas R_{AA} reveals the Cronin type enhancement with the peak at $p_T \approx 2$ GeV/c. The difference between R_{AA} and R_{CP} is striking, indicating significant enhancement of protons (in respect to p + p) for the $40 - 60\%$ collision centrality used in the definition of R_{CP} . The same misleading behavior of R_{CP} is seen for charged hadrons when comparing evolution of R_{AA} and R_{CP} on η for Au + Au at $\sqrt{s_{NN}} = 200$ GeV and $\sqrt{s_{NN}} = 62.4$ GeV [34].

Figure 13 shows the nuclear modification factors calculated for $(\pi^+ + \pi^-)/2$ (left panel) and $(p + \bar{p})/2$ (right panel), respectively, at $y \approx 3.2$, for central Au + Au reaction. For the comparison we plotted the R_{AA} measured by the PHENIX Collaboration at mid-rapidity. The R_{AA} measured for pions shows strong suppression (by factor of about 3 for $2 < p_T < 3$ GeV/c), both at mid and at forward rapidity. The consistency between mid and forward rapidity is seen also for protons, but in this case, R_{AA} reveals Cronin peak around $p_T = 2$ GeV/c. The similarity between R_{AA} at mid and forward rapidity observed

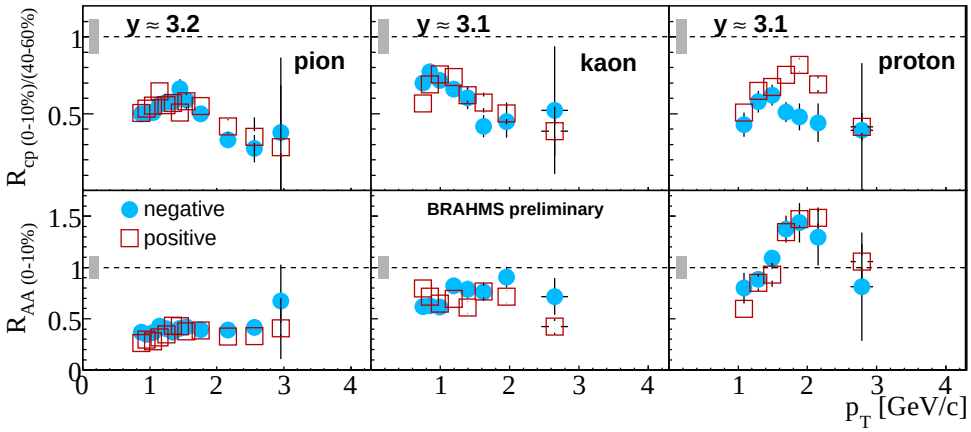

Figure 12. BRAHMS R_{AA} (upper row) and R_{CP} (bottom row) for pions, kaons and protons, measured $y \approx 3.2$ in Au + Au $\sqrt{s_{NN}} = 200$ GeV. The p + p reference was also measured by BRAHMS (see [35]).

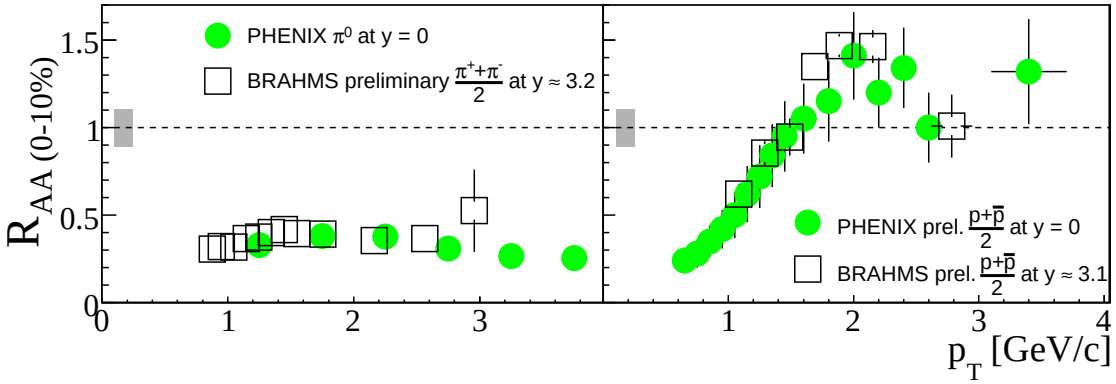

Figure 13. Comparison of R_{AA} measured for central Au + Au collisions at $\sqrt{s_{NN}} =$ 200 GeV, at mid-rapidity and $y \approx 3$ for pions (left panel) and protons (right panel).

simultaneously for pions and protons suggests the same mechanisms responsible for the nuclear modifications within the studied rapidity interval.

It has been predicted [36] that the magnitude of quenching should depend on size and density of the created absorbing medium, thus it is interesting to study the dependency of R_{AA} on centrality. In Figure 14 we plotted the averaged R_{AA} measured for pions versus the N_{part} for the mid-rapidity (squared shape symbols) and for forward rapidity (triangles). The averaging was performed in the p_T range from 2 GeV/c to 3 GeV/c. It is seen again, that for the most central Au + Au reaction, the mid and forward pion suppression is of the same strength. However, the R_{AA} measured at forward rapidity shows significantly stronger rise towards peripheral collisions as compared to R_{AA} at mid-rapidity, that leads to the discrepancy on the level of 35% for $N_{part} = 100$. The trend is consistent with the model of parton energy loss in strongly absorbing medium [37,38]. In this picture, for $y = 0$, the jet emission is dominated by the emission from the surface which quenches the dependence of R_{AA} on the system size. On the other hand, for $y \approx 3$, the transition from

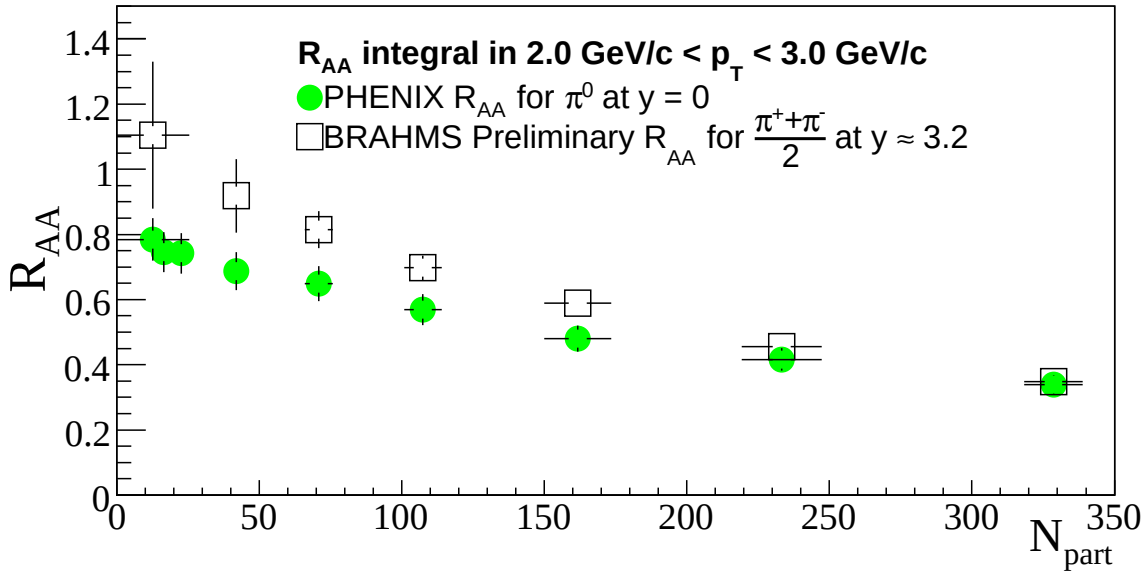

Figure 14. Averaged R_{AA} in the range $2.0 < p_T < 3.0$ GeV at mid rapidity (PHENIX) and at forward rapidity as a function of collision centrality, expressed by the number of participants.

surface to volume emission can occur, which leads to stronger dependency on N_{part} .

6. SUMMARY

The results from BRAHMS and other RHIC experiments clearly show that studies of high energy nucleus - nucleus collisions have moved to a qualitatively new physics domain. It is characterized by a high degree of reaction transparency leading to the formation of a near baryon free central region with approximate balance between matter and antimatter. From the measurement of charged particles multiplicieties in this region the lower limit for the energy density at $\tau_o = 1$fm/c have been determined which is 5 GeV/fm^3 and 3.7 GeV/fm^3, for central Au + Au reactions at $\sqrt{s_{NN}} = 200$ GeV and $\sqrt{s_{NN}} = 62.4$ GeV, respectively. Therefore the conditions necessary for the formation of a deconfined system appear to be well fulfilled for the RHIC energies. Analysis within the statistical model of the relative abundances of K^-, K^+, p and $\bar{p}$ suggests the equilibrium at chemical freeze-out at temperature of 170 MeV with the noticeably strong correlation between strange quarks and baryonic chemical potentials. The analysis of particle spectra within the blast-wave model indicates the kinetic freeze-out temperature of the order of 120 MeV and a large transverse expansion velocity which is consistent with the high initial energy density.

The measurement of the elliptic flow parameter v_2 versus rapidity and p_T shows weak dependence of the $v_2(p_T)$ on rapidity. The p/π ratios measured within $0 < \eta < 3$ for Au + Au and Cu + Cu at $\sqrt{s_{NN}} = 200$ GeV and $\sqrt{s_{NN}} = 62.4$ GeV reveal strong enhancement of protons and anti-protons yields compared to pion yields. The models that incorporate interplay between soft and hard proceses can discribe the data at mid-rapidity. We compared R_{AA} for Au + Au at $\sqrt{s_{NN}} = 200$ GeV and $\sqrt{s_{NN}} = 62.4$ GeV,

and for Au + Au and Cu + Cu at $\sqrt{s_{NN}} = 200$ GeV. The general observed trend is that R_{AA} increases with: decreasing collision energy, system size, and collision centrality. For Au + Au central collisions at $\sqrt{s_{NN}} = 200$ GeV the R_{AA} shows very weak dependence on rapidity (in $0 < y < 3.2$ interval), both for pions and protons.

7. ACKNOWLEDGMENTS

This work was supported by the division of Nuclear Physics of the Office of Science of the U.S. Department of Energy, the Danish Natural Science Research Council, the Research Council of Norway, the Polish Ministry of Science and Information Society Technologies grant number 0383/P03/2005/29 and the Romanian Ministry of Education and Research.

REFERENCES

1. C. Adler *et al.* [STAR Collaboration], Phys. Rev. C**66** 034904 (2002). J. Adams *et al.* [STAR Collaboration], Phys. Rev. Lett. **92** 062301 (2004).
2. S. S. Adler *et al.* [PHENIX Collaboration], Phys. Rev. Lett. **91** 182301 (2003).
3. P. F. Kolb and U. Heinz, nucl-th/0305084, and references therein.
4. B. B. Back *et al.* [PHOBOS Collaboration], nucl-exp/0407012 (2004).
5. I. Arsene *et al.* [BRAHMS Collaboration], Phys. Rev. Lett. **91** (2003) 072305.
6. D. Kharzeev, Y. V. Kovchegov, and K. Tuchin Phys. Lett. B599 (2004) 23, and references therein.
7. C. Adler *et al.* [STAR Collaboration], Phys. Rev. Lett. **90** 082302 (2003).
8. C. Adler *et al.* [STAR Collaboration], Nucl. Phys. A **715** 272 (2003).
9. I. Arsene *et al.* [BRAHMS Collaboration], Phys. Rev. Lett. **93** 242303 (2004)
10. J. Jalilia-Marian, Nucl. Phys. A **748** 664 (2005).
11. M. Adamczyk *et al.* [BRAHMS Collaboration], Nucl. Instr. and Meth. A **499** (2003) 437.
12. D. Kharzeev and E. Levin, Phys. Lett. B **599** (2001) 79.
13. I. G. Bearden *et al.* [BRAHMS Collaboration], Phys. Lett. B523 (2001) 227.
14. I. G. Bearden *et al.* [BRAHMS Collaboration], Phys. Rev. Lett. **88** (2002) 202301.
15. G. J. Alner *et al.*, Z. Phys. C**33**, 1 (1986).
16. J. D. Bjorken, Phys. Rev. D **27** (1983) 140.
17. I. G. Bearden *et al.* [BRAHMS Collaboration], submitted to Phys. Rev. Lett. (nucl-ex/0403050)
18. F. Karsch, Nucl. Phys. A **698** (2002) 199.
19. I. G. Bearden *et al.* [BRAHMS Collaboration], Phys. Rev. Lett. **93** (2004) 102301.
20. I. G. Bearden *et al.* [BRAHMS Collaboration], Phys. Rev. Lett. **90** (2003) 102301.
21. F. Becattini *et al.*, Phys. Rev. C**64** 024901 (2001).
22. P. J. Siemens and J. O. Rasmussen, Phys. Rev. Lett. **42** (1979) 808.
23. H. Ito [BRAHMS Collaboration], this volume.
24. C. E. Jørgensen *et al.* [BRAHMS Collaboration], Nucl. Phys. A **715** (2003) 741c.
25. Z. Yin *et al.* [BRAHMS Collaboration], J. Phys. G **30** (2004) S983.
26. R. J. Fries *et al.* Phys. Rev. C**68** 044902 (2003).
27. V. Greco, C. M. Ko, and I. Vitev, *et al.* Phys. Rev. C**71** 041901R (2005).
28. R. C. Hwa and C. B. Yang, Phys. Rev. C**70** (2004) 024905.

29. I. Vitev and M. Gyulassy, Nucl. Phys. A**715** (2003) 779c.
30. V. T. Pop *et al.*, Phys. Rev. C**70** (2004) 064906.
31. Eun Joo Kim [BRAHMS Collaboration], this volume.
32. T. Hirano, and Y. Nara Phys. Rev. C**68** (2003) 064902
33. X. N. Wang, Phys. Rev. C**58** 2321(1998).
34. T. M. Larsen [BRAHMS Collaboration], this volume.
35. R. Karabowicz [BRAHMS Collaboration], this volume.
36. M. Gyulassy, P. Levai, and I. Vitev, Nucl. Phys. B**594** (2001) 371. M. Gyulassy, P. Levai, and I. Vitev, Phys. Rev. D**66** (2002) 014005.
37. A. Dainese, C. Loizides, and G. Paić, Eur. Phys. J. C38 (2005) 461-474.
38. A. Drees, H. Feng, J. Jia, Phys. Rev. C**71** (2005) 034909.